Supporting Information for Nanoscale

Minimizing antibody cross-reactivity in multiplex detection of biomarkers in paper-based point-of-care assays

J.T. Dias, L. Lama, J.Gantelius and H.Andersson-Svahn*

Division of Proteomics and Nanobiotechnology, Science for Life Laboratory, KTH Royal Institute of Technology, Sweden. E-mail: helene.andersson.svahn@scilifelab.se; Tel: +46852480096

Characterization of AuNPs-Ab

- DLS and ζ -potential

DLS and ζ-potential measurements were performed on a Malvern Zetasizer Nano S90 instrument at 25°C. Each sample was diluted in assay buffer, except AuNPs, and was measured three times, combining 10 runs per measurement.

Figure S1 shows that the synthesized AuNPs have a hydrodynamic diameter of approximately 40 nm, as described by Bastús *et al*.[1]

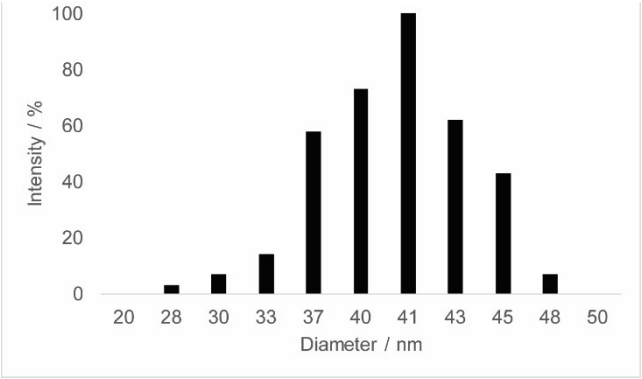

Figure S1: Hydrodynamic diameter of the AuNPs synthesized following the protocol described by Bastús *et al*. [1]

Coupling of the Ab to the AuNPs efficiency

Antibody overview

For this work three detection antibodies were chosen and purchased from Abcam. In table S1 is the information provided by the commercial supplier.

Table S1: Antibody description, type and catalog number.

Protein designation	Description	Catalog #	Type of Ab	Specificity
Epidermal growth factor (EGF)	Capture: Mouse monoclonal	ab18635	IgG1	Reacts with Human
	Detection: Goat polyclonal	ab9862	Unknown	Reacts with Human
Human EGF full length protein	-	ab55483	-	Human
Troponin-T (Trp-T)	Capture: Mouse monoclonal	ab8295	IgG1	Reacts with Mouse, Rat, Dog, Human
	Detection: Mouse monoclonal	ab10223	IgG1	Cow, Human
Cardiac Troponin T full length protein	-	ab9937	-	Human
Interleukin-2 (IL-2)	Capture: Mouse monoclonal	ab38151	IgG2a	Reacts with Human
	Detection: Goat polyclonal	ab1075	IgG	Reacts with Human, mouse
Active human IL2 full length protein	-	ab73598	-	Human

By measuring the ζ-potential in three different stages of the modification protocol; after the gold nanoparticle synthesis, after the coupling of PEG-COOH and after the coupling of the antibody, it was possible to infer if the surface of the nanoparticles was indeed being modified (Table S2).

Table S2: ζ-potential measurements performed for nanoparticles prior to functionalization (AuNPs), PEG modified nanoparticles (AuNPs-PEG-COOH) and antibody modified nanoparticles (AuNPs-PEG-Ab) presented as the mean of 10 runs ± standard deviation.

	ζ-potential (mV)
AuNPs	-36.3 ± 1.3
AuNPs-PEG-COOH	-12.8 ± 2.1
AuNPs-PEG-Ab	-21.7 ± 2.3

The ζ-potential of the AuNPs-PEG-Ab were carried out for the sample where the gold nanoparticles were coupled with the EGF antibody.

The AuNPs obtained by the citrate capping method (Turkevich method[1]) are negatively charged due to the presence of the citrate outer layer. PEG molecules are neutrally charged, thus when introduced to the surface of the nanoparticles it will affect the net charge of the constructs. Removing citrate ions and replacing them with PEG molecules results in a decrease of the negativity of the nanoparticles. The antibodies used in this work are predominantly negatively charged at the pH of the assay buffer. Hence, when coupled to the nanoparticles and the ζ-potential measured at pH 7.4, confer negative charge to the constructs. The increased negativity observed when the Abs were coupled to the AuNPs-PEG-COOH shows that antibody molecules were introduced onto the surface of the nanoparticles.

The concentration of Ab coupled to the AuNPs was quantified indirectly by determining the concentration of Ab recovered in the washing steps. As a control for nonspecific interactions between Ab and AuNPs a coupling protocol was carried out without activation of the carboxyl groups with EDC. The quantification was carried out using the Bradford protein assay. Table S3 shows that for each Ab (EGF; Trp-T and IL-2) the coupling efficiency was within 64 and 83%. These values indicate that the coupling protocol allowed the construction of AuNPs-Ab. For each Ab studied the nonspecific interaction was below 10%, thus such interactions were considered to be negligible.

Table S3: Coupling efficiency in percentage for the three Ab that were modified onto the surface of AuNPs. The efficiency is obtained by quantifying, through a Bradford protein assay, the excess of Ab that was unable to bind to the AuNPs.

	Coupling efficiency (%)	Ab:AuNPs
AuNPs-PEG-EGF	82.6 ± 2.6	17 ± 2
AuNPs-PEG-TrpT	75.2 ± 4.1	20 ± 1
AuNPs-PEG-IL2	63.8 ± 8.6	21 ± 1

Cross-reactivity characterization

The different sets of AuNPs-PEG-Ab were mixed and allowed to incubate for 1h at room temperature. Non-specific interactions between the different antibodies were expected and were studied with dynamic light scattering (DLS) measurements. The EGF-AuNPs, TrpT-AuNPs and IL2-AuNPs independent solutions were also analyzed. It was observed that when these three constructs are not mixed with each other, a single population of nanoparticles was in solution (Figure S2 A-C). However, when mixed the size distribution dispersity increases (Figure S2 D-G) and such was observed for all possible mixed combinations of constructs. One can infer that the increment of size distribution is somewhat related to the interaction between the different antibodies. Although it is not a direct assessment of possible cross-reactivity, it is likely that the size dispersity increment associated with Ab-Ab interactions.

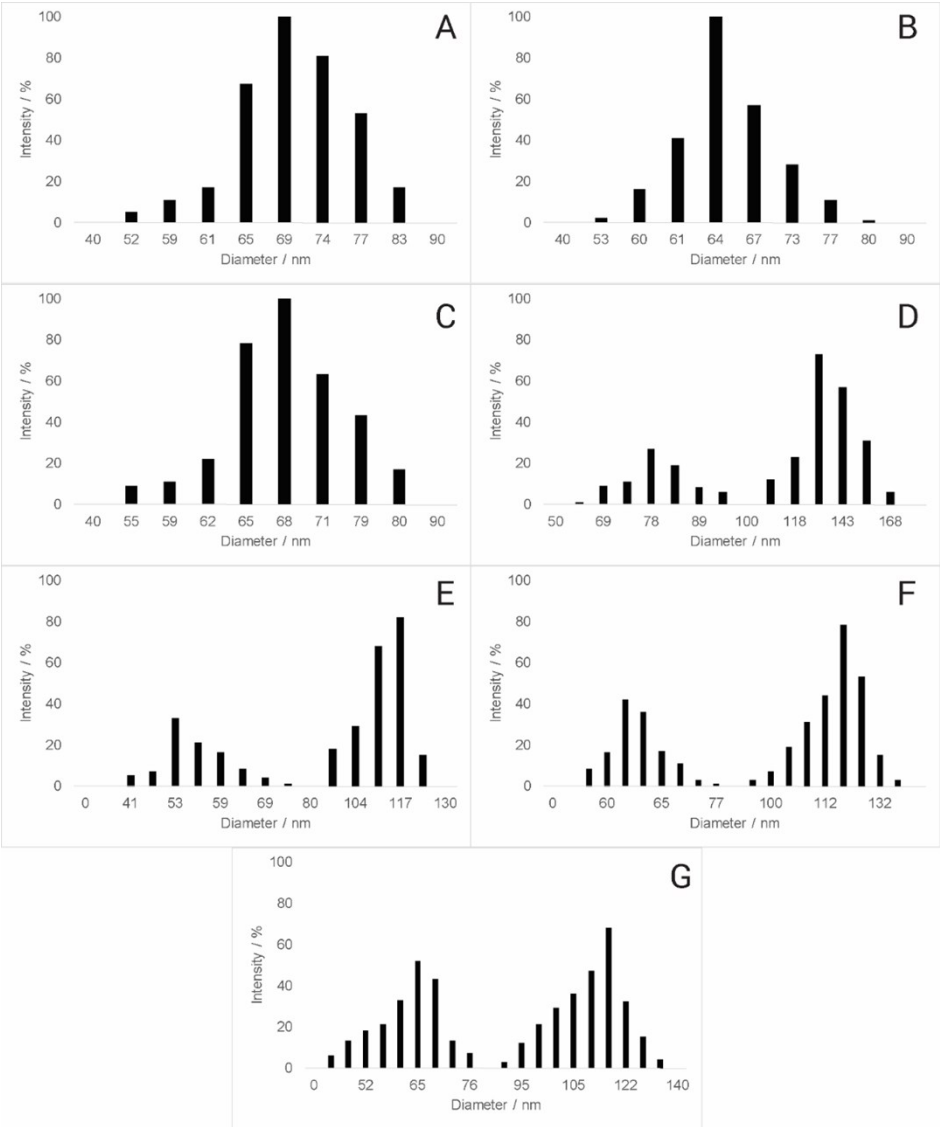

Figure S2: Hydrodynamic diameter of the AuNPs modified with: (**A**) EGF antibody; (**B**) Trp-T antibody and (**C**) IL-2 antibody. (**D**) mix of all three antibody modified; (**E**) mix of EGF-AuNPs and Trp-T-AuNPs; (**F**) mix of EGF-AuNPs

and IL-2-AuNPs; (**G**) mix of Trp-T-AuNPs and IL-2-AuNPs. Each sample was diluted in water at pH 7 and was measured three times, combining 10 runs per measurement.

Moreover, assays were carried out where a single antigen (Figure S3 A-C) was to be detected and combinations of two antigens (Figure S3 D-E) were to be detected. The detection was carried out with a mix of the three Ab-modified AuNPs without prior ultrasound application. No non-specific detection was observed, the combination of both lack of availability of the antibodies for detection, due to non-specific interactions between Ab-modified AuNPs, and the speed of the flow of the detection Ab-AuNPs mix through the vertical flow setup unables those semi-aggregated constructs to interact with the antigens on the array.

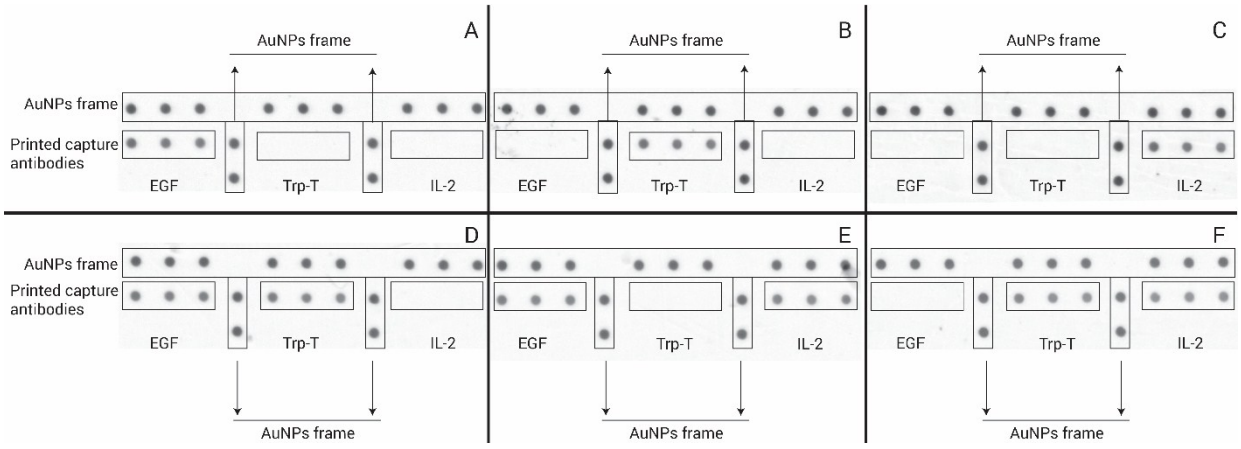

Figure S3: Assays where a solution containing 50 ng.mL^{-1} of a single antigen was to be detected with the mix of detection Ab-modified AuNPs: (**A**) Only EGF antigen was flown; (**B**) only Trp-T antigen was flown and (**C**) only IL-2 antigen was flown; and solution containing 50 ng.mL-1 of two antigens was flown prior to be detected with the mix of detection Ab-modified AuNPs; (**D**) EGF and Trp-T antigens were flown; (**E**) EGF and IL-2 antigens were flown and (**F**) Trp-T and IL-2 antigens were flown.

DLS measurements of the Ab-AuNPs mix after ultrasound application were carried out. The DLS technique has proven to be reliable in size determination of monodisperse colloidal solutions. However, for polydisperse colloids such measurements can be faulty. In general terms, the DLS technique relies on an autocorrelation curve obtained from the fluctuating scattering intensity. Each particle in solution contributes to the total scattering intensity with a factor proportional to its square weight. This autocorrelation can, to an extreme, mask small objects by the presence of bigger ones. As shown by Tomaszewska et. al[2], multiple narrow peak detection is highly dependent on the ratio of the particles in solution and their relative size. And even if the percentage of a larger community of nanoparticles is small, the intensity of the DLS peaks will be greater than the smaller community. Such problem is also address by most manufactures of DLS apparatus in the troubleshooting section of the equipment's manual.

In the case of the samples here reported, the DLS measurements before (Figure S4A) and after ultrasound is applied (Figure S4B) show no significant difference. If the DLS is measured 1h after the application of the ultrasound, the profile of the size histogram maintains its resemblance to the sample before application of ultrasound.

One might interpret the data as the ultrasound application produced no effect in minimizing the nonspecific interactions between the different Ab-AuNPs in the mix. However, this explanation is not corroborated by

the results obtained when the detection assays were carried out. A significant difference between the samples that were sonicated and those that were not was observed.

A more reasonable explanation for similar DLS histograms can be the fact that the contribution of the larger particles (nonspecific interacting Ab-AuNPs) in solution to the scattering intensity is most likely masking the one from the smaller particles (non-interacting Ab-AuNPs), inducing the observer to conclude that no effect was achieved with the ultrasound application.

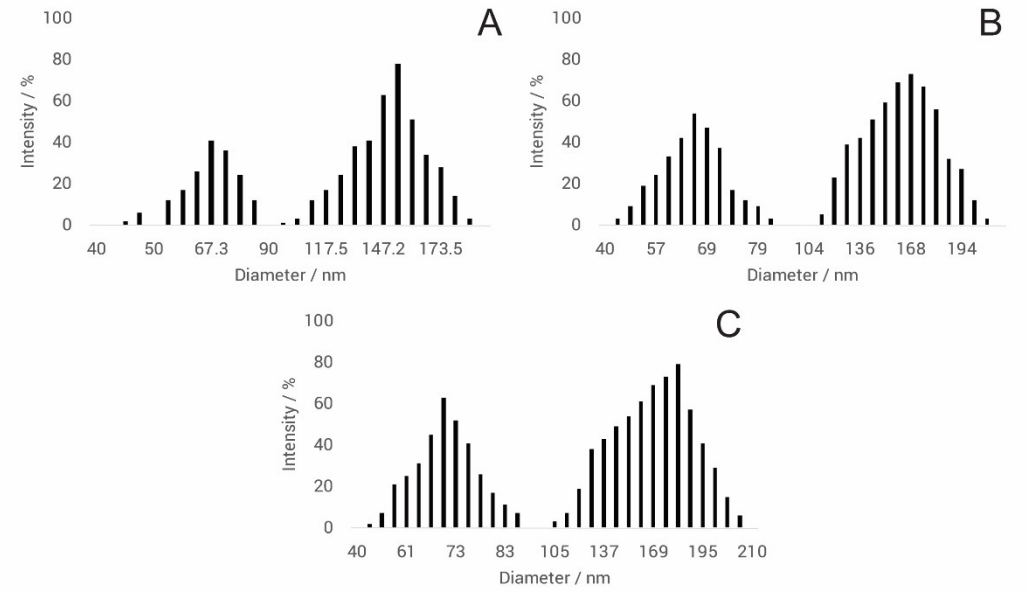

Figure S4: Hydrodynamic diameter of the (**A**) detection Ab-AuNPs mix prior to the application of ultrasound; (**B**) immediately after the application of the ultrasound and (**C**) 1h after the ultrasound was applied.

Limit of detection and quantification

The limit of detection, LOD, has been defined by international organizations such as ISO, IUPAC and ICH.[3] For non-instrumental analytical validation, the recommendations are the analysis of a sample with known concentration of analyte. A minimum concentration at which the analyte can be reliably detected needs to be established.[4] A standard curve of the known concentrations plotted against the measured intensities allows to determine the slope (*s*). Both *s* and the standard deviation (*SD*) calculated for the minimum concentration that the analyte can be detected (in this report that concentration was determined to be 5 pg.mL^{-1} for all three antigens studied) are to be applied in equation 1:

Equation (1): $$LOD = \frac{3.3 \times SD}{s}$$

For the limit of quantification, LOQ, the recommendations are to use a factor of 10 instead of 3.3 in equation 1, thus the LOQ can be calculated according to equation 2:

Equation (2): $$LOQ = \frac{10 \times SD}{s}$$

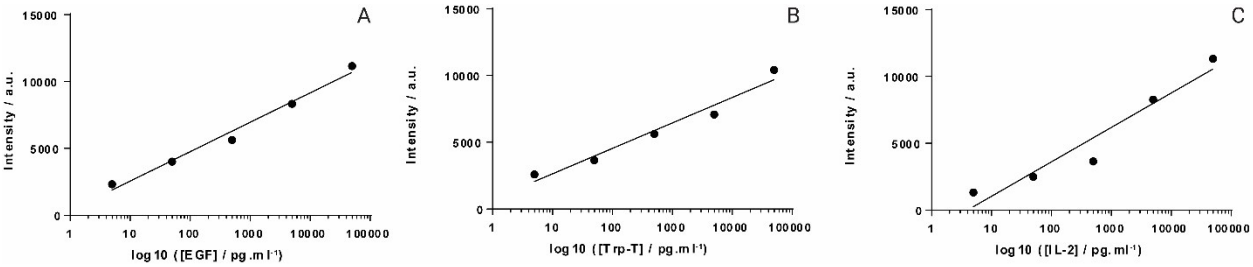

Figure S5: Measured spot intensities plotted against the log 10 concentration of (**A**) EGF antigen, (**B**) Trp-T antigen and (**C**) IL-2 antigen.

With the slope of each standard curve (Figure S5 and table S4) and the SD attained for the lowest concentration detected (5 pg.mL^{-1}), both LOD and LOQ were calculated for the three antigens (Table S4).

Table S4: Limit of detection, limit of quantification and coefficient of variation (%) calculated for the detection of the three antigens.

Antigens	%CV	Standard Dev. (SD)	Slope (s)	R square	LOD (pg.mL^{-1})	LOQ (pg.mL^{-1})
EGF	3.8	536.7	2200	0.9825	0.81	2.30
Trp-T	1.1	700.8	1906	0.9610	1.21	3.68
IL-2	3.3	872.9	2579	0.9299	1.12	3.75

In figure S6 it is possible to observe no detection spots when no antigen is flown. The values obtained through ImageJ analysis of the array where approximately zero in all cases. Thus, it was considered that the background intensity would have a value of zero.

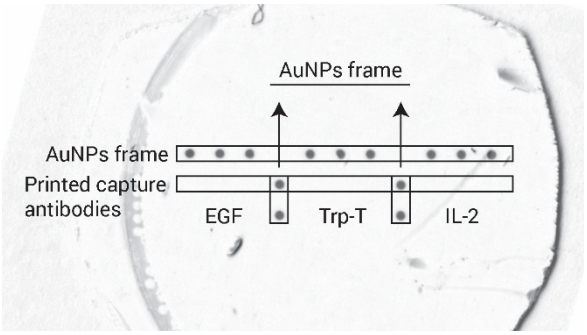

Figure S6: Assay where no antigen was flown prior to flowing the detection Ab-modified AuNPs mix. Apart from the visible spots from the printed AuNPs frame no other spot is observed in these conditions.

Consideration of forces involved in AuNPs-Ab – AuNPs-Ab interaction

Previous reports have shown that ultrasonic energy can promote de-agglomeration of AuNPs.[5,6] In this work, it was hypothesized that applying ultrasonic energy to the mix containing the several detection Ab-AuNPs would minimize nonspecific cross-reactivity events.

Atomic force microscopy (AFM) studies have given a measure of the range of the forces that are necessary to overcome the potential energy in the bonds between protein-ligand pairs. It has been reported that the forces required to separate Ab pairs interacting either specific and nonspecifically are in the pN range.[7,8,9] The AFM technique typically requires one of the interacting biomolecules to be immobilized. In our system the Ab-AuNPs interact with each other while free in solution. A model that describes the nonspecific cross-reactivity between Ab-AuNPs is to the best of our knowledge yet to be proposed.

The nonspecific interactions can occur mainly electrostatically (particle on particle interaction), molecularly (antibody on antibody interaction) or by adsorption to the AuNPs (antibody on particle interaction).

To study the forces acting on the AuNPs and Ab-AuNPs generated by the ultrasound probe a model of the setup was simulated using COMSOL Multiphysics®. The velocities of the fluid in different points in the solution could be extracted from the simulation and used to calculate hydrodynamic drag forces acting on the particles. For the setup used in our work it was hypothesized that the forces in the sample in the vicinity of the probe along with differences in the velocity gradients are expected to minimize nonspecific interactions.

Repulsive electrostatic forces between charged AuNPs

The repulsive electrostatic force between AuNPs is assumed to be significantly larger than the Brownian interactions between the AuNPs and was modeled as described by Zou *et al*.[10] The electrostatic pair interaction is expressed as in equation S3 and it was modeled with the parameters described in table S4 and S6. The Debye length, defined in equation S4, is the length scale in meters of the electrostatic interactions surrounding the particles.

$$F_{Electrostatic}(s) = \frac{64\pi r C_0 N_A k_B T \Gamma^2}{\kappa} e^{-\kappa s} \qquad (Equation\ S3)$$

$$\kappa^{-1} = \sqrt{\frac{\varepsilon_0 \varepsilon_r k_B T}{2 N_A C_0 e^2 z^2}} \qquad (Equation\ S4)$$

Table S6: Description of parameters in equations S3 and S4.

Symbol	Description	Unit	Value
r	Particle radius	m	$20 \cdot 10^{-9}$
C_0	Electrolyte concentration in solution	$mol\, m^{-3}$	450
N_A	Avogadro's number	mol^{-1}	$6.022 \cdot 10^{23}$
k_B	Boltzmann constant	$J\, K^{-1}$	$1.38 \cdot 10^{-23}$
T	Temperature	K	297
ε_0	Vacuum permittivity	$F\, m^{-1}$	$8.85 \cdot 10^{-12}$
ε_r	Dielectric constant of the solvent		80.4
e	Elementary charge	C	$1.602 \cdot 10^{-19}$
z	Valence of an electrolyte		1

The electrostatic repulsive forces between the AuNPs in three different cases; particle on particle interaction, antibody on antibody interaction, and antibody on particle interaction are shown in table S4. For the antibody on antibody and antibody on particle interactions it was assumed an antibody length of 8.5 nm.[11] It was determined that, for the scenarios where interactions occur through Ab, the electrostatic repulsion forces are considerably smaller than those resulting from the applied ultrasound (Table S7). This corroborates our findings as the application of the ultrasound force showed to greatly improve detection.

Table S7: The electrostatic repulsion force between constructs in the three different combinations possible.

	Electrostatic force (N)	Separation distance, s (nm)	Surface potential, Γ (mV)
AuNP – AuNP	$5.2 \cdot 10^{-13}$	0.28	– 21.7
Ab-AuNP – Ab-AuNP	$7.3 \cdot 10^{-29}$	17	– 21.7
Ab-AuNP – AuNP	$8.4 \cdot 10^{-21}$	8.5	– 21.7

Forces acting on AuNPs due to acoustical radiation

The forces required to reverse the formation of AuNPs-Ab agglomerates must be large enough in size and direction to overcome the bonds formed between the AuNPs-Ab. In general, the total force from an acoustical field acting on a particle is the sum of the radiation force and the Stokes drag force originated by the induced acoustic streaming flow.[12] Acoustical radiation forces have shown to affect different sized particles to different extents. For particles in the nano scale the acting forces are mainly dominated by the Stokes drag force.[13] The Stokes drag force for AuNPs with 40 nm in diameter modified with Ab (with a length of approximately 8.5 nm) was determined using equation S5.

$$F_d = 6\pi\mu r v \qquad (Equation\ S5)$$

The velocity values, v, were obtained from a simulation of the experimental setup made in COMSOL Multiphysics®, which include the ultrasonic probe homogenizer acting on the sample. The value of the dynamic viscosity, μ, for water at room temperature of $1.003 \cdot 10^{-3}\ Pa \cdot s$ was considered.

A 2 dimension rotationally symmetric COMSOL Multiphysics® simulation was made on 1 ml of sample in a 1.5 mL Eppendorf® Flex Tube®. The fluid in the sample was modeled as water with an electrolyte concentration of 0.45 M, bulk viscosity of $3.09 \cdot 10^{-3}\ Pa \cdot s$ and speed of sound $1494\ m/s$ in the fluid at 24°C.[14] The pressure acoustics module in the frequency domain was used to model a viscous fluid with a negative inward acceleration at the probe tip. The inward acceleration is given in by the second time derivative of the displacement in the frequency domain and is presented in equation S6.

$$a = \int d_0(i\omega)^2 e^{i\omega t} dt = d_0(i\omega)^2 \qquad (Equation\ S6)$$

Where d_0 is the amplitude of the ultrasonic wave. The SONOPLUS Ultrasonic Homogenizer mini 20 (BANDELIN) with a Micro Tip MS 1.5 (3639) probe used in this work allowed a maximum wave amplitude of 90% of $65\ \mu m$. The value of the complex angular frequency, $i\omega$, is given by COMSOL®.

The mesh was calibrated for fluid dynamics, and a predefined extremely fine mesh was used to give accurate values of the velocities close to the probe.

The simulation was run for an acoustical wave frequency of $30\ kHz$ as performed by the mini20. The power was derived from the simulation to compare with the experimental value. The velocity values at different location points in the tube were also obtained and are presented in table S6. The surface integral over the 1D probe radius allows the calculation of the total power output from the probe surface (Equation S7). Applying equation S7 to our system, the calculated total power was of 1.3 W.

$$P = \iint \frac{p^2}{2\rho c} dA = \int \frac{p^2}{2\rho c} 2\pi r_{probe}\, dr \qquad (Equation\ S7)$$

where ρ and c is the density and speed of sound of the fluid, p is the pressure amplitude at the probe, and r_{probe} is the radius of the probe.

The mini20 homogenizer allows the power to be set at 2.0 W. However, when simulating the output power by the probe (Equation S7) the actual value will be approximately 1.3 W for our settings.

The velocities of the fluid induced by the acoustic field were obtained from the expression of the local velocity, v_{rms}, in COMSOL®. The velocities on a 2D surface of the Eppendorf® tube were applied to the Stokes equation (equation S5) to obtain the values of the forces acting on the Ab-AuNPs in different point locations in the tube. The radius that was used to calculate the forces is the combined AuNPs plus Ab length, resulting in a total radius of $28.5\,nm$. Figure S7 show the 2D plot of the velocity in the tube that is rotationally symmetric.

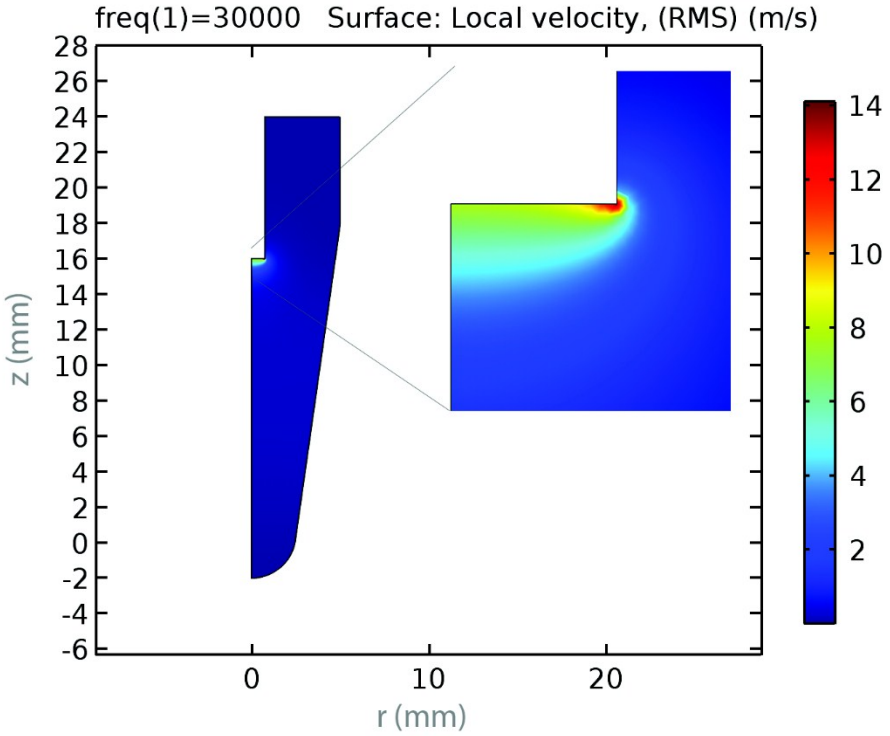

Figure S7: 2D plot of the velocities predicted by COMSOL®. The highlighted section shows the position of the tip of the probe, where the velocity is at its maximum. The center of the probe is located at 0 and has a radius of 0.75 nm.

Table S8 shows the velocities and forces that our model predicts for the setup used in this work. According to the COMSOL® simulation, the local maximum velocity of the probe used in our system is of $20.4\,m/s$ with an average value of $8.99\,m/s$. The value for the average velocity in the vicinity of the probe tip yields a force of approximately 4.8 nN on the Ab-AuNPs.

Table S8: Velocities and forces in our system predicted by COMSOL®. Values of the velocities are extracted along the probe and in the whole solution.

	Velocity (m/s)	Force (pN)
Probe maximum	20.4	11
Probe average	8.99	4.8
Probe minimum	7.80	4.2
Solution maximum	20.4	11
Solution average	0.19	0.1
Solution minimum	$3.85 \cdot 10^{-6}$	0.002

However, the drag forces revealed by the COMSOL® simulation are not in themselves sufficient to allow Ab-AuNPs de-agglomeration. For such event to occur, the gradients of velocities on the particles need to be pointed in different directions as depicted in figure S8.

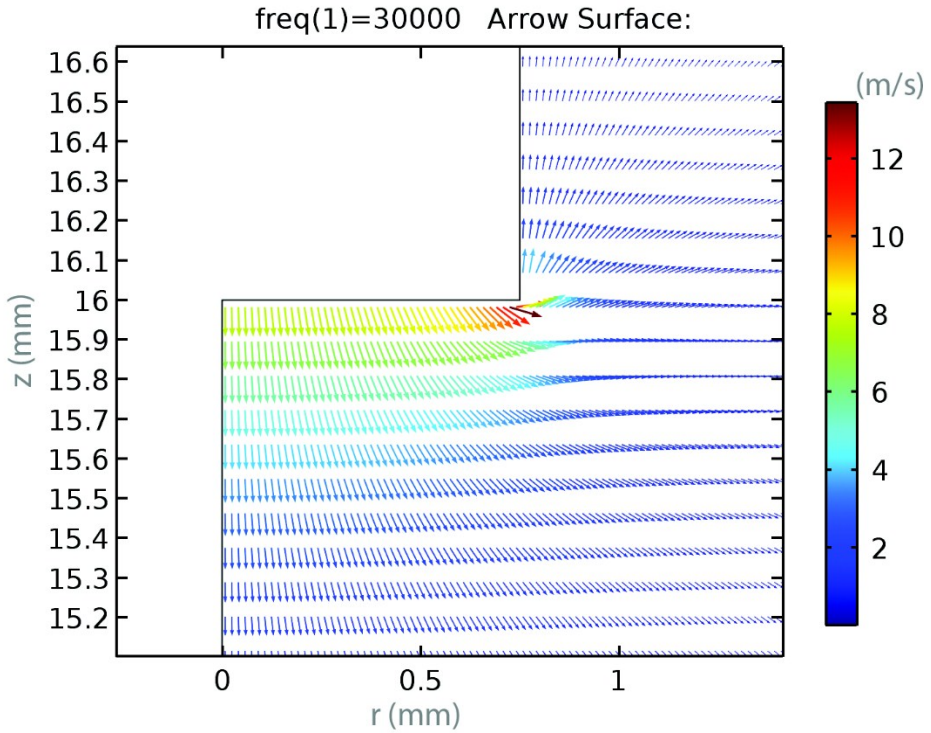

Figure S8: The velocity gradient field in the vicinity of the probe. The lengths of the arrows are drawn logarithmically to the velocity gradient size. The colors of the arrows show the velocity value in that point.

The gradient field of the velocity is represented as an arrow field with the colors corresponding to the velocity value. The higher velocity gradient field can be observed in the vicinity of the probe. These gradients become smaller and more uniform as we move away from the probe. The velocities predicted at the edge of the probe indicate that this is the solution's area where the Ab-AuNPs will be most prone to de-agglomeration. Thus, to investigate the maximal differential hydrodynamic force between two adjacent particles, a mesh with minimum element size of 25 nm was used to obtain velocity values at a separation of 50 nm. The differential hydrodynamic force in a line $\pm 0.01\ mm$ from the edge of the probe, where the smaller mesh was applied, was obtained with an average value of 400 pN and a minimum value of 8 pN.

The application of ultrasound promotes the movement of the Ab-AuNPs in solution. The particles that at some point in time are in areas with small and uniform velocity gradients will, at a given time, enter an area where the velocity gradients are higher. It is in these high velocity gradient areas where the de-agglomeration of nonspecific cross-reacting Ab-AuNPs most likely occurs. Such de-agglomeration can justify the difference in detection limits observed between the assays where ultrasound was applied and those where no ultrasound was carried out.

Another physical phenomenon promoted by the ultrasound application is the production of cavitation activity. This is the formation of gas-filled bubbles.[15] The changes in pressure due to the ultrasound waves promotes the expansion and contraction of these bubbles. This will originate oscillations in the bubble size that ultimately create a circulating fluid flow termed microstreaming.[16]

Cavitation activity has been described to occur over the whole ultrasound frequency range.[17] The formation of these cavitating bubbles can be considered to promote the flow of the Ab-AuNPs in solution, thus aiding the circulation of the Ab-AuNPs between low and high velocity gradient areas of the Eppendorf®.

References

1.N. G. N. Bastús, J. J. Comenge, and V. V. Puntes, *Langmuir*, 2011, **27**, 11098–11105.

2.E. Tomaszewska, K. Soliwoda, K. Kadziola, B. Tkacz-Szczesna, G. Celichowski, M. Cichomski, W. Szmaja, and J. Grobelny, *J Nanomater*, 2013, **2013**, 1–10.

3. *Validation of Analytical Procedures: Methodology*, 2009.

4.A. Shrivastava and V. Gupta, *Chron Young Sci*, 2011, **2**, 21.

5.K. Okitsu, M. Ashokkumar, and F. Grieser, *J Phys Chem B*, 2005, **109**, 20673–20675.

6.O. Jakobsson, C. Grenvall, M. Nordin, M. Evander, and T. Laurell, *Lab Chip*, 2014, **14**, 1943–1950.

7.M. Hegner, C. Gerber, Y. Arntz, and J. Zhang, *J Chromatogr Lib*, 2003, **68**, 241–274.

8.E. Celik and V. T. Moy, *J Mol Recognit*, 2011, **25**, 53–56.

9.C.-K. Lee, Y.-M. Wang, L.-S. Huang, and S. Lin, *Micron*, 2007, **38**, 446–461.

10.H. Ben-Yoav, P. H. Dykstra, W. E. Bentley, and R. Ghodssi, *Biosens Bioelectron*, 2014, **64**, 579–585.

11.V. R. Sarma, E. W. Silverton, and D. R. Davies, *J Biol Chem,* 1971.

12.J. T. Karlsen and H. Bruus, *Phys Rev E*, 2015, **92**, 043010.

13.R. Barnkob, P. Augustsson, T. Laurell, and H. Bruus, *Phys Rev E*, 2012, **86**, 056307.

14.M. Greenspan, *The Journal of the Acoustical Society of America*, 1959, **31**, 75.

15.S. B. Barnett, G. R. Ter Haar, M. C. Ziskin, W. L. Nyborg, K. Maeda, and J. Bang, *Ultrasound in Medicine & Biology*, 1994, **20**, 205–218.

16.W. L. Nyborg, *Br J Cancer Suppl*, 1982, **5**, 156–160.

17.W. G. Pitt, G. A. Husseini, and B. J. Staples, *Expert Opinion on Drug Delivery*, 2004, **1**, 37–56.